NPS-PH-91-006

NAVAL POSTGRADUATE SCHOOL

Monterey, California

SEA TEST DEVELOPMENT OF LASER ALTIMETER

E. C. Crittenden, Jr., G. W. Rodeback,
E. A. Milne, and A. W. Cooper

January, 1991

Final Report
For Period October 1988-December 1990

Prepared for:
Postgraduate School
rey, CA 93943

NAVAL POSTGRADUATE SCHOOL

RADM R. W. West
Superintendent

Dean H. Schull
Provost

This research was performed for the Naval Sea System Command, Sea 06W31 and was funded with O. & M. N. direct funding by the Naval Postgraduate School

This report was prepared by:

UNCLASSIFIED
SECURITY CLASSIFICATION OF THIS PAGE

REPORT DOCUMENTATION PAGE

1a. REPORT SECURITY CLASSIFICATION Unclassified	1b. RESTRICTIVE MARKINGS
2a. SECURITY CLASSIFICATION AUTHORITY	3. DISTRIBUTION / AVAILABILITY OF REPORT Approved for public release distribution unlimited
2b. DECLASSIFICATION / DOWNGRADING SCHEDULE	
4. PERFORMING ORGANIZATION REPORT NUMBER(S) NPS-PH-91-006	5. MONITORING ORGANIZATION REPORT NUMBER(S)
6a. NAME OF PERFORMING ORGANIZATION Naval Postgraduate School 6b. OFFICE SYMBOL (If applicable) Dept PH	7a. NAME OF MONITORING ORGANIZATION
6c. ADDRESS (City, State, and ZIP Code) Monterey, CA, 93943-5000	7b. ADDRESS (City, State, and ZIP Code)
8a. NAME OF FUNDING / SPONSORING ORGANIZATION Naval Postgraduate School 8b. OFFICE SYMBOL (If applicable)	9. PROCUREMENT INSTRUMENT IDENTIFICATION NUMBER O.&M.N. Direct Funding
8c. ADDRESS (City, State, and ZIP Code) Monterey, CA, 93943-5000	10. SOURCE OF FUNDING NUMBERS PROGRAM ELEMENT NO / PROJECT NO / TASK NO / WORK UNIT ACCESSION NO

11. TITLE (Include Security Classification)
Sea Test Development of Laser Altimeter, (Unclassified)

12. PERSONAL AUTHOR(S)
E.C.Crittenden,Jr., G.W.Rodeback, E.A.Milne, and A.W.Cooper

13a. TYPE OF REPORT	13b. TIME COVERED	14. DATE OF REPORT (Year, Month, Day)	15. PAGE COUNT
Final	FROM 1989 TO 1990	1991, January	24

16. SUPPLEMENTARY NOTATION

17. COSATI CODES			18. SUBJECT TERMS (Continue on reverse if necessary and identify by block number)
FIELD	GROUP	SUB-GROUP	Laser Altimeter, Sea Surface Reflectance, Vertical reflectance, Narrow beam laser reflectance.

19. ABSTRACT (Continue on reverse if necessary and identify by block number)

Low altitude (81 m.) narrow-beam laser reflectance measurements were made from the nearly ocean-like water surface under the Golden Gate bridge. This site allowed precise measurements not possible from flying platforms. For short wavelength water waves superimposed on swell, the signal amplitude probability distribution showed periods of zero return signal, even for vertical incidence, apparently due to tipping of the average water surface. The nonzero signals show an antilog-normal probability distribution, skewed toward higher signal than that provided by a normal (Gaussian) distribution. With incidence angle displaced from the vertical, the distribution shape is retained but with more frequent zero reflections. The decrease with angle of the average signal, including the zeroes, is well fitted with a Gram-Charlier distribution, as seen by earlier observers using photographic techniques which masked these details of the structure. For the simpler wave pattern due to a long sustained wind direction, the signal amplitude probability distribution is log-normal with no zero signal periods. For this case, the distribution shifts toward

20. DISTRIBUTION / AVAILABILITY OF ABSTRACT ☒ UNCLASSIFIED/UNLIMITED ☐ SAME AS RPT ☐ DTIC USERS	21. ABSTRACT SECURITY CLASSIFICATION Unclassified
22a. NAME OF RESPONSIBLE INDIVIDUAL A. W. Cooper	22b. TELEPHONE (Include Area Code) (408) 646-2452 22c. OFFICE SYMBOL PH/CR

DD FORM 1473, 84 MAR 83 APR edition may be used until exhausted
All other editions are obsolete

SECURITY CLASSIFICATION OF THIS PAGE

☆ U.S. Government Printing Office: 1986—606-24.

UNCLASSIFIED

Block 19, continued:
exponential at large angles from the vertical. For surface states intermediate between the above two extremes the distribution is often normal. The larger return signals resulting from the skew toward larger amplitudes from lognormal are more favorable for disposable laser altimeters than previously believed. Also for an altimeter which may be swinging from a parachute or balloon, the return at angles from the vertical remains high. The presence of occasional zero return signal does degrade the accuracy of altitude somewhat for a descending altimeter, but the signal available assures performance at larger altitudes than previously expected.

SUMMARY

In this continuing program a small disposable laser altimeter developed earlier in the program was used to measure the reflected signal from the sea surface as represented by the waters beneath the Golden Gate Bridge. The work revealed a number of new features of the reflection not previously reported elsewhere. The bridge was used as a site both because the cost of helicopter, airplane or blimp platforms would have been prohibitive and because sampling sequences at precise angles from the vertical would have been difficult to achieve from such platforms. Thirty-second samples of the return signal were taken at a one kilohertz rate at each of a number of angles from the vertical in the upwind and crosswind directions, during twelve separate occasions on the bridge. The probability distribution for the frequency of occurrence of return signals as a function of signal amplitude showed interesting new structure. In the presence of swell superimposed on a shorter wavelength pattern, periods of zero return signal occur, even for vertical incidence. This is apparently due to tipping of the reflection scatter-cone of the smaller waves far enough from the vertical that no light is reflected vertically. The probability distribution of the nonzero signals in this situation has a shape that can be fitted with an antilog-normal distribution. This is skewed toward higher signal than that provided by a normal (Gaussian) distribution. When the incidence angle is displaced from the vertical, the distribution shape stays the same but the zero reflections become more frequent. The average signal, including the zeroes, falls off with angle. The variation of the average signal as a function of angle is well fitted with a Gram-Charlier distribution, the same as found earlier by other observers using photographic techniques which did not reveal these details of the structure. The Gram-Charlier distribution is somewhat more peaked than Gaussian in both the crosswind and up/downwind direction. In the up/downwind direction it is slightly skewed upwind. For the simpler wave pattern produced by a single long sustained wind direction, the probability distribution of the signal amplitude is log-normal and no periods of zero reflection occur. For this situation the distribution shifts from lognormal toward exponential as the angle from the vertical is increased. At large angle the distribution is well fitted by an exponential curve. For intermediate surface states, with a mixture of waves of different amplitudes and different directions, but in the absence of large swell, the distribution is usually intermediate between lognormal and antilog-normal, being normal in some cases. The overall behavior of the reflection is more favorable for disposable laser altimeters than previously believed because the skew toward higher amplitudes gives frequent large signals. higher amplitudes. Also for an altimeter which may be swinging from a parachute or balloon, the return at angles from the vertical remains high. The presence of occasional zero return signal does degrade the accuracy of altitude somewhat for a descending altimeter, but the enhanced signal due to the distribution skew improves performance at larger altitudes.

TABLE OF CONTENTS

LIST OF FIGURES

I. INTRODUCTION

The work reported here provides detailed information on the nature of the reflection from ocean-like waves for narrow beam laser altimeters or similar devices. The work was a continuation of a project[1] in which a small, light, rugged, and inexpensive disposable laser altimeter was developed for parachute or balloon-borne use over the ocean. In such a device, laser power, detector sensitivity and signal-to-noise considerations dictate use of as narrow a laser beam and detector field of view as possible. In the course of field tests it became apparent that narrow laser beam reflection from ocean-like water waves was different from that previously reported for wide angle laser or radar beam reflection. The reflection was found here to be more favorable for narrow beam laser altimeters than for the log-normal probability distribution of intensity that is generally assumed. The results indicate that a log-normal distribution is applicable to wide angle beams, or for narrow beams with short wavelength water waves in the absence of long-wavelength swell. For narrow beams, and complex wave patterns, including swell with wavelength several times the laser spot width, the results show distributions that are often normal, or antilog-normal, i.e. skewed from normal in the direction of high intensity, opposite to that for log-normal. For these latter distributions , the reflection is often zero for periods up to a few tenths of a second, even in the vertical direction. As the incident angle is varied from the vertical, the frequency of zero reflection increases, but the probability distribution of the nonzero part of the reflections usually does not change its shape. The average intensity, including the zero reflections, does fall off with angle and follows the well established Cox and Munk[2], (Gram Charlier[3]) distribution, but the peak probability of finite signals usually remains unchanged. This behavior is favorable for laser altimeters, because the returned signal is larger than anticipated on the basis of a log-normal distribution. Swinging of the beam direction is also less of a problem than expected because the signal magnitude remains constant with angle. Some loss of precision in height determination is present for an altimeter that is changing altitude, because of the occasional absence of a return signal for several tenths of a second. This may be a negligible, or a significant, problem depending on the rate of change of altitude of a package carrying a laser altimeter.

II. EXPERIMENTAL TECHNIQUE

The measurements were made from the center of the Golden Gate bridge at a height of 81 meters above the water at average high tide. Measurements were made at high tide slack to provide clean ocean water without tidal flow. The waves often included a long wavelength swell from the west, a shorter wavelength set of waves from a different direction from earlier wind, and shorter wind-driven waves due to the wind at the time.

A five-element GaAs laser array was used, with a peak power output of about 50 watts and half power pulse time of about 150 nanoseconds, pulsed at a rate of 1 kiloherz. The beam was formed to a rectangular cone with divergence of 0.3 by 0.4 degrees with an f/1.5 anastigmatic and coma corrected 39 mm diameter uncoated two-element lens. This provided a 42 by 57 cm image of the emitting five-element array on the water. The receiver was an identical lens imaging the water spot onto a circular avalanche Si detector so as to have an angular acceptance in the form of a circular cone of full angle 0.5 degrees.

The system was aligned on a horizontal laboratory range of 81 meters length (the same length as the bridge height) so that the receiver accepted the return from the complete laser pattern. A 10 nanometer band-width multilayer filter covered the receiving lens to reduce the noise due to sunlight scattered from the water, while passing about 60% of the laser signal. Because the laser output power varied strongly with temperature, it was calibrated as a function of temperature, using a thermocouple mounted on the laser mounting flange. The Si detector was essentially temperature independent.

In order to relate the water reflectance to Lambertian reflectance, the system was calibrated by measuring the return signal from a 73% reflectance Lambertian cardboard surface on the 81 meter laboratory range immediately before and after measurements from the bridge.

On the bridge, the combined laser and receiver "optical head" was mounted on a rod extending out over the water from the rail of a small meteorological platform outside the west bridge walkway. The optical head was provided with a quick-acting screw-driven goniometer to permit scanning in two perpendicular directions from the vertical, with the scanning planes set by a third angular positioner. The bridge lies nearly north and south (7 degrees west of north).

The "optical" sea state at the time of a vertical reflectance measurement was determined by measuring the size of the elliptical "glitter" pattern. This pattern was measured by scanning the optical head in angle, usually up to 10 degrees from the vertical, or until the average return signal was reduced by a factor of about 3. A sequence of reflected returns was recorded in the vertical direction, then a set of such sequences recorded for

each of a number of angles scanning in one plane. Then the vertical sequence was repeated, followed by a scan in a plane perpendicular to the first plane, and then a final vertical reading. The proper directions for scanning in the directions of the major and minor axes of the elliptical glitter pattern were determined by visual observation of the principal water waves and in case of doubt, with some preliminary scans. For some runs the wave patterns were also recorded with a video camera and recorder. Since the initial and final vertical measurements often did not repeat well, due to changes in the water wave pattern, the intervening data were adjusted assuming linear variation with time.

The Golden Gate bridge has girder structures beneath the roadway which interfered with scanning from positive to negative angles except for scans parallel to the bridge. Consequently, half-scan sequences were used to characterize the "optical" sea-state in most cases.

The data sampling was restricted by two considerations; a need for long data trains to get good statistics, and a need to take the data in a short enough period of time to avoid changes in the wind and consequent wave pattern. The longest period fluctuations occurred because of swells with periods of the order of 10 seconds. This dictated data runs of a number of swell periods. The compromise chosen was data runs of 30 seconds with 30,000 data points. With this data train length, a complete scan in two planes took about 10 minutes. In many cases the reflection was fairly constant over this period. In others, variations in vertical reflectance as large as a factor of two sometimes occurred, necessitating linear adjustment with time of the readings between each pair of vertical readings.

The received return signals were pulse-stretched and held in a sample-and-hold circuit, then digitized and stored in electronic memory of a portable computer. This data was then transferred to hard disk storage during the approximately 5 second interval in which the angular position of the head was changed.

Preliminary data processing was carried out on the bridge with the portable computer in order to provide a basis for adjustment of the receiver system gain and laser power. This was necessary to prevent the occurrence of signals so large as to saturate the receiver or the digitizer, or too low to be reliable. The data was processed by computer later in the laboratory, yielding plots of frequency of occurrence vs. received signal voltage. The average return signal, including the zero amplitude returns, was also calculated. In some cases saturation of the receiver or digitizer did occur, leading to a false spike at the high end of the distribution curves. The error due to this never exceeded 1.5%, so it has been neglected.

III. RESULTS

1. Small Waves Without Swell.

Three distributions from a sequence of five scans ranging from vertical to 8 degrees from the vertical are shown in Figs. 1 to 3. The probability shown there is the probability of falling in a bin of 1/41 of a volt in width. The water surface had no large swells and was characterized by small waves of wavelength about the size of the laser spot, plus smaller ripples. Fig. 1 shows the distribution for the vertical direction, Fig. 2 shows the distribution for 4 degrees from the vertical, and Fig 3., 8 degrees from vertical. The shape of the distribution curve for the vertical direction is roughly log-normal. As the angle from the vertical is increased, the resemblance to a log-normal distribution decreases. At large angles from the vertical, the shape becomes suggestive of exponential. There is no distinctly separate zero reflection spike in any of the distributions, with zero reflection occurring only at fairly large angle as part of a general shift toward lower signal amplitude with increasing angle from the vertical.

For general comparison of distribution types, four ideal distribution functions are shown in Fig. 4. These are: exponential, log-normal, normal (Gaussian), and antilog-normal.

For the exponential distribution:

$$Y = Y_0 \exp\{-X/X_1\} ,$$

for the log-normal distribution:

$$Y = Y_0 \exp\{-[\ln(X)-\ln(X_1)]^2/2\sigma^2\} ,$$

for the normal distribution:

$$Y = Y_0 \exp\{-[X-X_1]^2/2\sigma^2\} ,$$

and, for the antilog-normal distribution:

$$Y = Y_0 \exp\{-[\exp(X)-\exp(X_1)]/2\sigma^2\} .$$

The vertical signal distribution shown in Fig. 1, for the vertical direction, is replotted in Fig. 5 for comparison with a log-normal distribution. A three-parameter nonlinear least square fit was employed to match the log-normal curve to the data. The parameters are the signal value at peak probability, the magnitude of the peak probability, and the standard deviation of the associated normal distribution function. The curve representing the experimental data in that figure has been smoothed by doubling the bin-width in calculating the distribution curve.

The distribution shown in Fig 3 for 8 degrees from the vertical, is replotted in Fig. 6 for comparison with an exponential distribution. A two-parameter least square fit was employed for matching, using as parameters, Y_0, the Y intercept, and X_1, value of X for $Y = Y_0/e$. The first four points, plotted as diamonds in Fig. 4, have been omitted in the fitting process. The fit to the remainder of the curve is remarkably close.

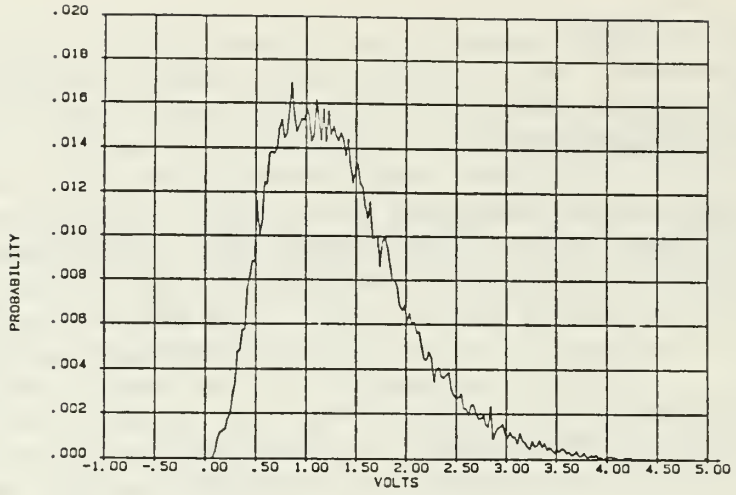

Fig. 1 Probability distribution for the return signal from waves without swell, straight down.

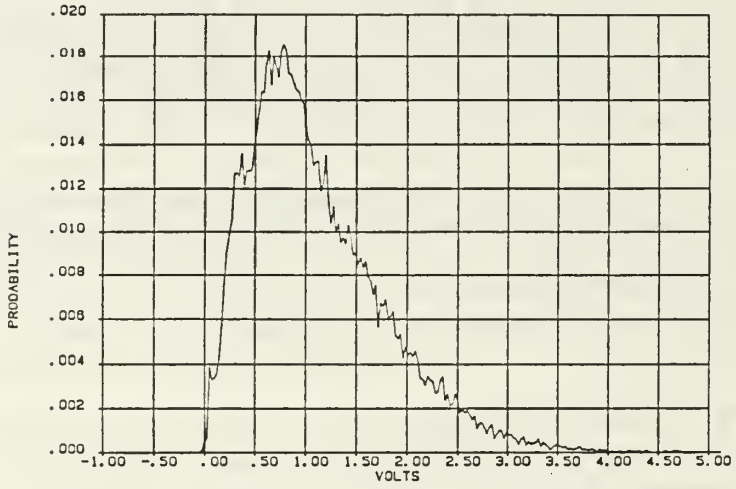

Fig. 2 Probability distribution for the return signal from waves without swell, 4 degrees from the vertical.

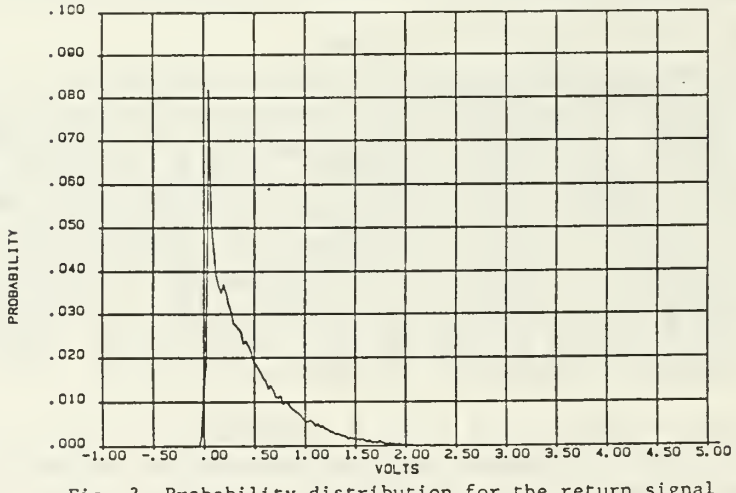

Fig. 3 Probability distribution for the return signal from waves without swell, 8 degrees from the vertical.

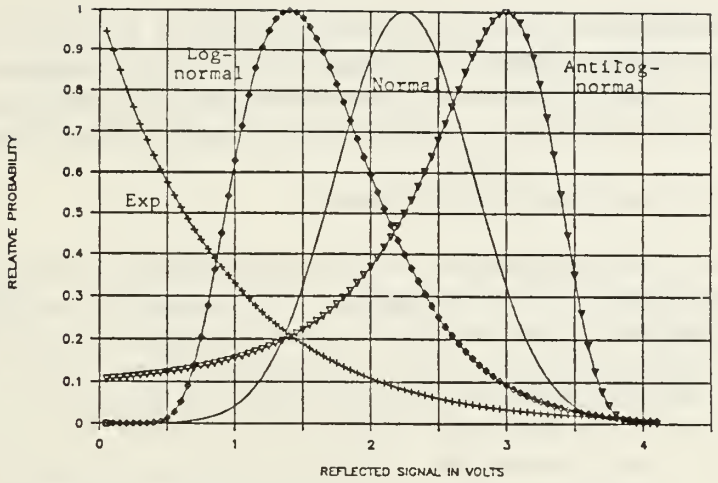

Fig. 4 Exponential, log-normal, normal, and antilog-normal distributions

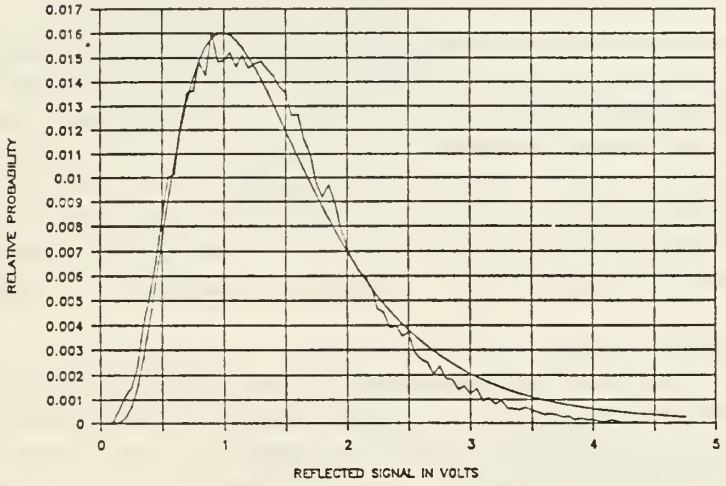

Fig. 5 Log-normal curve fitted to the distribution of Fig. 1.

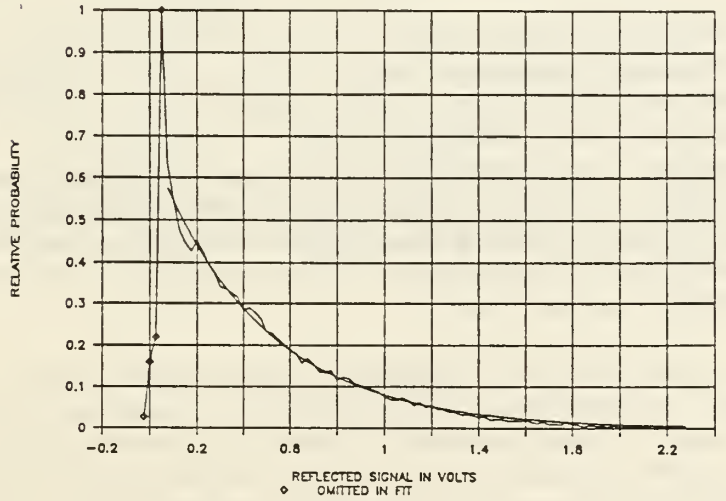

Fig. 6 Exponential curve fitted to the distribution of Fig. 3.

Distributions similar to those shown in Figs 1 to 3 were seen in many cases, and were associated with small waves in the absence of long wavelength swell. This is presumably the situation that would apply for a wide angle radar or laser beam or at high altitude for narrow beam systems.

2. Waves in the Presence of Swell.

The behavior is quite different for the case of long wavelength swells plus smaller wind driven waves and ripples. The smaller waves may be moving in the same direction as the swells or in quite a different direction. In the presence of swells, periods of zero reflection occur that persist for times from a few milliseconds up to several tenths of a second. Fig. 7 shows a time sequence of the reflected pulse amplitude for the vertical direction. The length of time covered by that figure is short because the 1000 hertz pulse rate prevents resolving individual pulses if a longer period is shown.

A set of curves for the reflectance with a large swell running is shown in Figs. 8, 9, and 10. The three distributions are part of a set of taken at eight different angles from the vertical. The vertical scales are different in the three curves because the magnitude of the zero reflectance peak changes through a large range. An important feature of Figs. 8 to 10 is that the signal value at the peak probability, and the curve profile, do not change with angle from the vertical. However, the average signal does change because the peak at zero reflectance changes with angle.

Two distribution curves from a set taken immediately after Figs. 8 to 10, but scanned in a plane perpendicular to that for Figs 8 to 10, are shown in Figs. 11 and 12. The shape of these curves is the same as for those of Figs. 8 to 10. They also show the important features of retaining the same signal value for peak probability and the same shape at all angles from the vertical.

The shape of the non-zero portion of the curves of Figs. 8 through 12 is suggestive of an antilog-normal curve. In Fig. 13 an antilog-normal curve has been least-squares fitted to the data of Fig. 8, for vertical reflection, excluding the zero reflection peak. The experimental curve has been somewhat smoothed by doubling the bin width. Although the fit is imperfect, the shape is definitely suggestive of antilog-normal. Such a distribution, that is skewed toward larger signal than for a log-normal distribution, is favorable to operation of a laser altimeter device because the maximum probability signal is larger.

The behavior with large long wavelength waves superposed on shorter wavelength waves, regardless of their relative directions, is qualitatively consistent with a model in which a small reflected cone from the short wavelength waves is rocked back and forth so as to fall outside the detector for part of the time. This leads to occurrence of periods of zero reflection at all angles from the vertical. It also leads to distributions

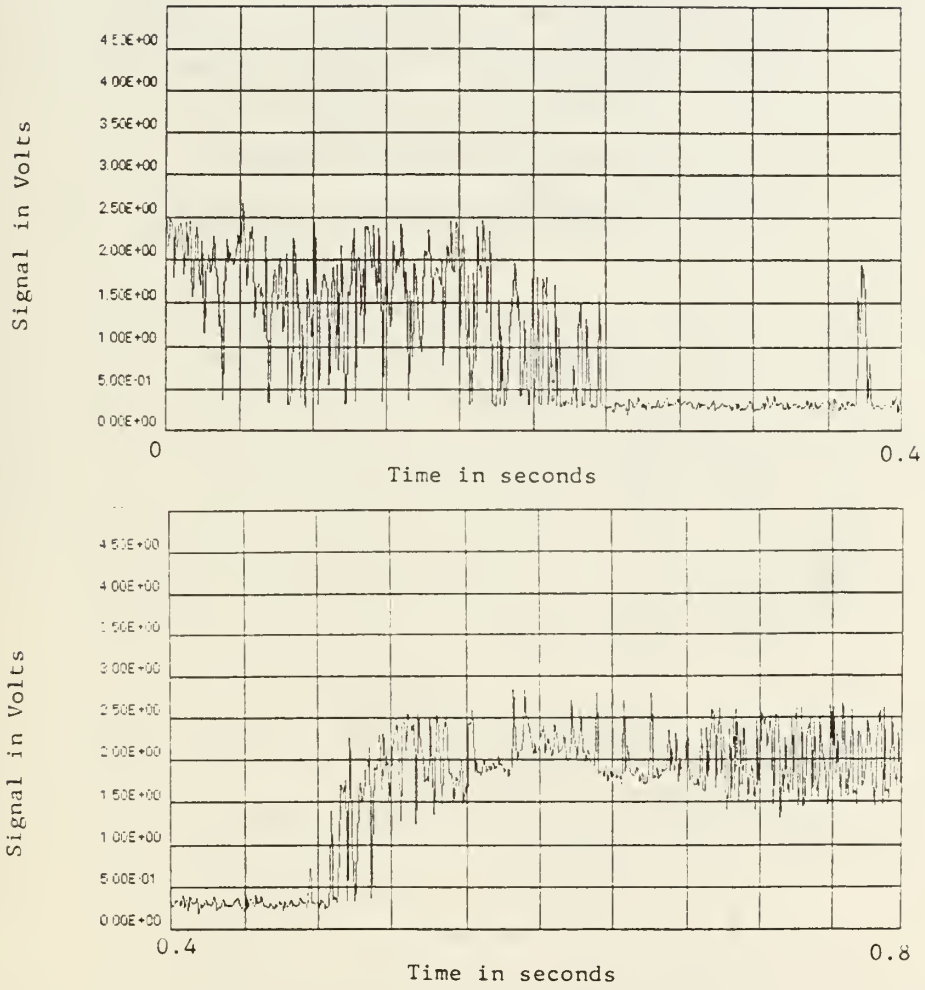

Fig. 7 Return signal as a function of time for the run with probability distribution shown in Fig. 8. The zero is offset vertically by about 0.3 volts in this figure, permitting display of the noise when zero signal is present.

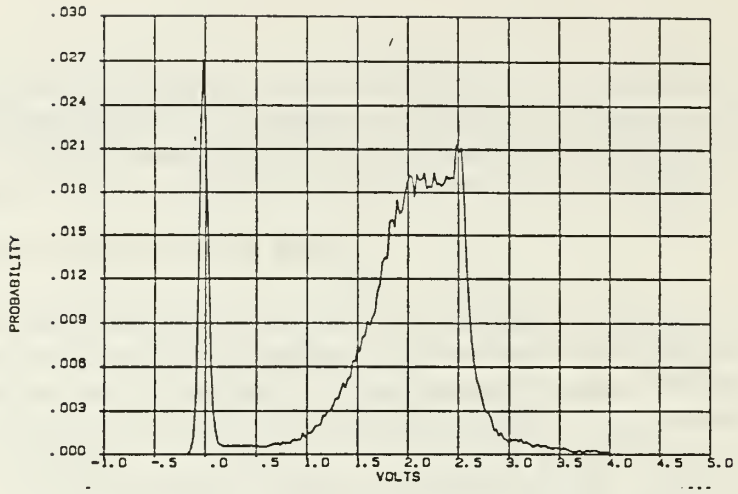

Fig. 8 Probability distribution for return signal for waves superposed on large swell, viewed straight down.

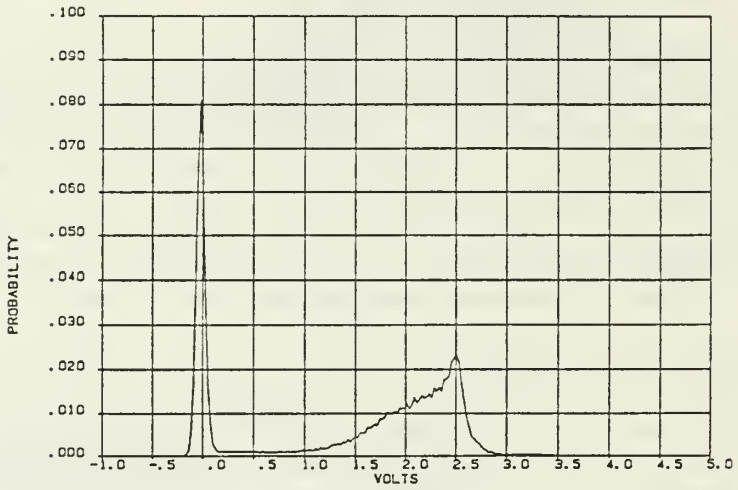

Fig. 9 Probability distribution for return signal for waves superposed on large swell, viewed 6 degrees from the vertical.

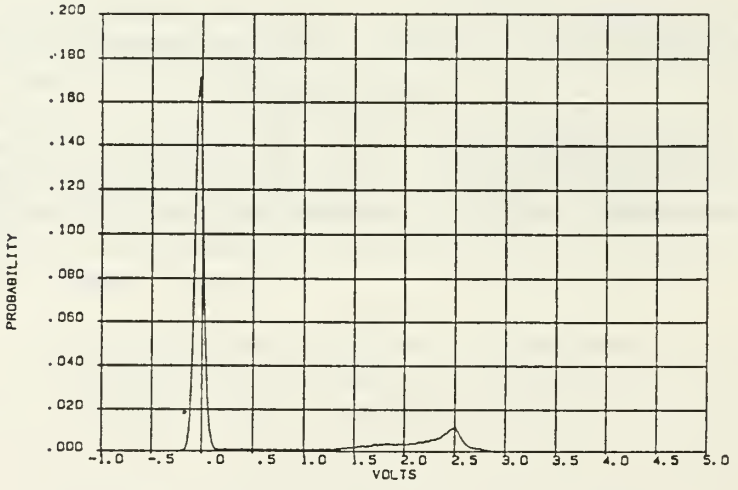

Fig. 10 Probability distribution for return signal for waves superposed on large swell, viewed 12 degrees from the vertical.

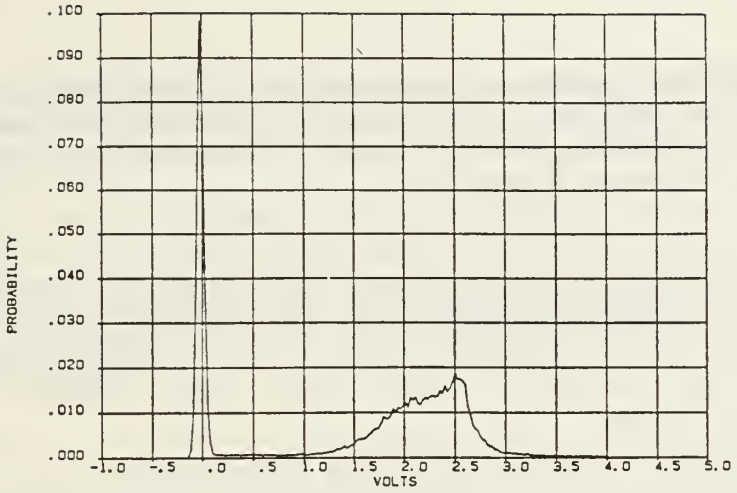

Fig. 11 Probability distribution for return signal for waves superposed on large swell, viewed 6 degrees from the vertical, in plane perpendicular to that of Figs. 8 to 10.

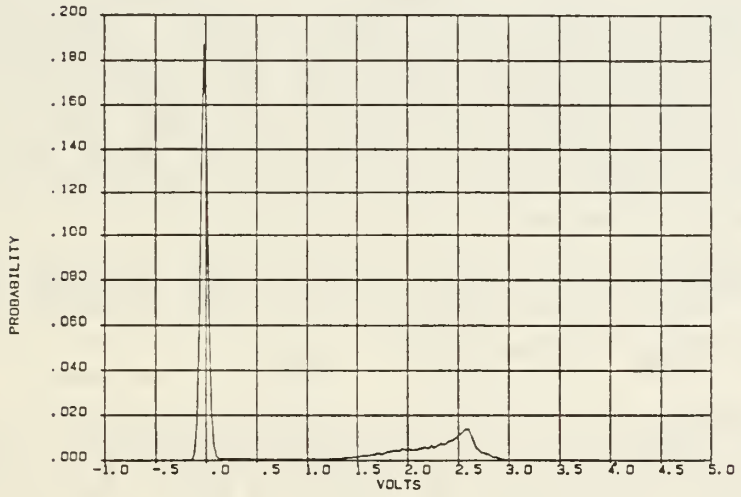

Fig. 12 Probability distribution for return signal for waves superposed on large swell, viewed 10 degrees from the vertical, in plane perpendicular to that of Figs. 8 to 10.

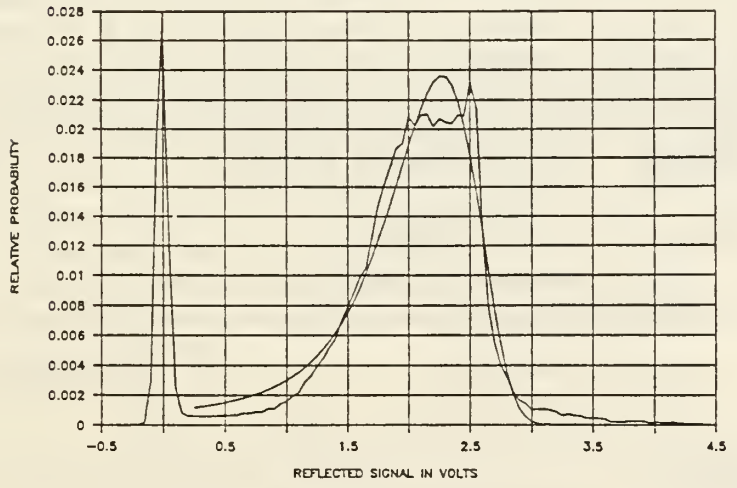

Fig. 13 Antilog-normal curve fitted to the distribution of Fig. 8.

that are similar to antilog-normal and are approximately constant with angle from the vertical. As the amplitude of long wavelength waves decreases, the distribution shifts toward a log-normal distribution, and the disappearance of periods of zero signal.

Most of the data taken on the Golden Gate bridge were for cases where the water-wave structure included some long wavelength swells. The data usually showed probability distribution curve shapes intermediate between those of Figs 1 to 3 and Figs 8 through 12, in the general region of normal distribution. In most cases the distribution shapes remained constant with angle from the vertical.

Several features of these distributions are favorable for laser altimeter operation. For complex water wave patterns the distributions deviate from log-normal toward normal or beyond, to antilog-normal, yielding an increase in the most probable nonzero signal value. This means that a required threshold signal will occur at a larger altitude. Additionally, the near constancy of distribution with angle from the vertical, for complex water surfaces, reduces the problem of adequate signal for a swinging laser altimeter. The average signal does decrease with angle from the vertical because of the increased frequency of zero return signal, but the frequency of occurrence of large signals remains high. The occurrence of intervals of a few tenths of a second in which the signal is zero will introduce some error in altitude for a descending altimeter, but the most probable signal magnitude is larger than what would be predicted from the average signal.

3. Average Signal as a Function of Angle.

The angular distribution of reflected signal was measured by Cox and Munk[2] to determine the distribution of wave surface angle as a function of wind velocity. They photographed the reflection glitter pattern from the sun from high altitudes to obtain a distribution of average intensity with angle. Their data was taken from an aircraft at high altitude over the open ocean, with the surface wind velocity recorded on a support ship below. For the sun as a source, the illumination is at a constant angle. As a result, the average intensity in the reflected glitter pattern subtends angles that are twice the wave slope distribution. Cox and Munk found their data for the wave slope distribution to be well fitted by a Gram-Charlier[3] distribution. This distribution is as follows:

$$G = [1/(2\pi\sigma r_u \sigma_c)] \times \exp\{-(X^2+Y^2)/2\} \times$$
$$[1 - (1/2)\, C_{21}(X^2-1)Y - (1/6)C_{03}(Y^3-3Y)] \quad \leftarrow \text{Skew}$$
$$+ (1/24)C_{40}(X^4-6X^2+3)$$
$$+ (1/24)C_{04}(Y^4-6Y^2+3)$$
$$+ (1/4)\, C_{22}(X^2-1)(Y^2-1) + \ldots] \quad \left.\right| \text{ Peakedness (Kurtosis)}$$

Or for simplicity:

$$G = [1/(2\pi\sigma_u\sigma_c)] \times \exp\{-(X^2+Y^2)/2\} \times [H]$$

The first two terms in the above expression, preceding the bracket, [H], represent a normal, or Gaussian, distribution in two dimensions,

Where: $X = \Theta/\sigma_u$,

with Θ the angle from the vertical in the up/downwind direction,

and: $Y = \Phi/\sigma_c$

with Φ the angle from the vertical in the crosswind direction,
and σ_u and σ_c the standard deviations in the up/downwind and crosswind directions respectively.

The up/downwind and crosswind Gram-Charlier distributions are plotted in Fig. 14, for a wind velocity of 10 meters per second, to illustrate the distinction between up/downwind and crosswind. A Gaussian distribution is included for comparison.

The up/downwind cross-section in the Gram-Charlier model is skewed, whereas the crosswind cross-section is not. Both functions are somewhat more peaked than the Gaussian. For the crosswind distribution the peak is a constant 11% above the Gaussian, independent of the wind velocity. For the up/downwind cross-section the peak is slightly skewed to one side of center and the peak is slightly higher than for the crosswind, depending on wind velocity.

The glitter patterns encountered in this work were all nearly circular, apparently because several different wave patterns were running at the same time. For such glitter patterns the distinction between the up/downwind direction and the crosswind disappears. In these cases the data for average reflected intensity as a function of angle from the vertical was reduced by fitting a crosswind Gram-Charlier curve to the data points. The fitting was done by a nonlinear regression analysis, i.e. minimizing the sum of the squares of the deviations from the Gram-Charlier function, while varying both the vertical average intensity and the sigma value. This yielded a best-fit value of sigma and the average vertical reflected intensity.

In a few data runs the wind direction and a principal set of waves was well established. In this case the up/downwind Gram Charlier function was used to obtain best-fit values for sigma and the average vertical intensity. This was accomplished by a three parameter nonlinear regression analysis. The values of sigma and vertical reflected intensity were varied to minimize the sum of the squares of the deviations to obtain sigma values for the crosswind and up/downwind variation of signal with angle. Then Cox and Munk's relationships between the sigma values and the wind velocity, W,

$$\sigma^2 = .003 + 5.12 \times 10^{-3} W$$

$$\sigma^2 = \sigma_u^2 + \sigma_c^2$$

were used to get a preliminary value of W. This value of W was then used to get values of the constants C_{21} and C_{03} by the Cox and Munk relationships:

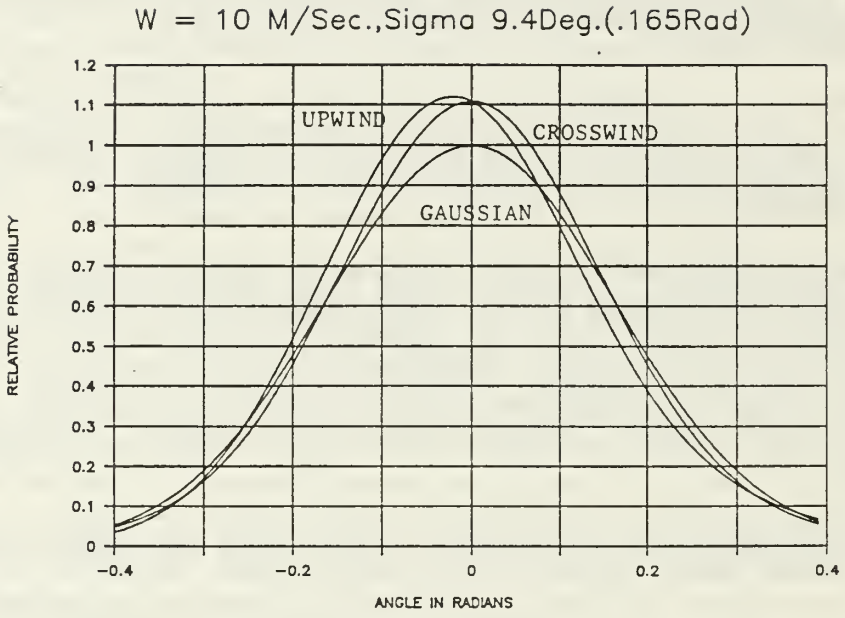

Fig. 14 Gram-Charlier distribution for wind speed of 10 m/sec.

$C_{21} = .01 - 0.0086W \pm 0.03$

$C_{03} = 0.04 - 0.033W \pm 0.12$

The process was repeated until the sum of the squares of the deviations reached a minimum. This usually occurred in about five cycles.

Fig. 15 shows the data points and the fitted Gram-Charlier function for the average intensity values for the sequences from which Figs 8 to 10 were taken. Fig 15 was fitted by means of the up/downwind function. In this case of large sigma and small associated inferred wind velocity the distinction from the crosswind function is almost imperceptible.

4. Central Reflected Intensity.

For illumination by a point source near the receiver, which was done in the experiments reported here, the angular distribution of the average reflected intensity has the same distribution as the wave slope distribution. (For a source such as the sun, the angular spread is doubled.) The Gram-Charlier distribution was used here, with this angular difference included, to interpret the data on the average reflected intensity distribution.

The expected intensity of the average returned reflection signal for the vertical direction can be calculated by utilizing the fact that the energy impinging on the water surface is returned into a cone that has twice the angle, or 4 times the solid angle, of the observed glitter pattern for a point source at the receiver. Assuming that this cone has an intensity cross-section given by twice the Gram-Charlier function in each angular direction, the return reflected power received by unit area at the detector will be:

$$F_G = (1/4)rP\ \{1/2\pi\sigma_u\sigma_c\}[H_o]/R^2$$

where r is the reflectivity of the water surface at near normal incidence, P is the power output of the laser, R is the distance from the laser and receiver lenses to the water surface, and $[H_o]$ is the Gram-Charlier function [H] for zero angle from the vertical.

For comparison, a "perfectly rough" or Lambertian surface which reflects equally in all directions within a hemisphere, but with the reflectivity, r, of water, will return a power per unit area to the detector of:

$$F_L = rP/\pi R^2$$

Consequently, ρ, the ratio of the actual wind ruffled water surface reflection to that for a water Lambertian surface would be:

$$\rho = F_G/F_L = [H_o]/8\sigma_u\sigma_c = 1.11/8\sigma_u\sigma_c$$

Measured values of ρ are compared with the predicted values in Fig 16. The curve is plotted as a log-log plot because the values encountered cover too large a range for reasonable plotting on a linear scale. That the points lie nearly on a line of unity slope indicates that the results are consistent with Cox and Munk's results. Although 30 angular sequences were

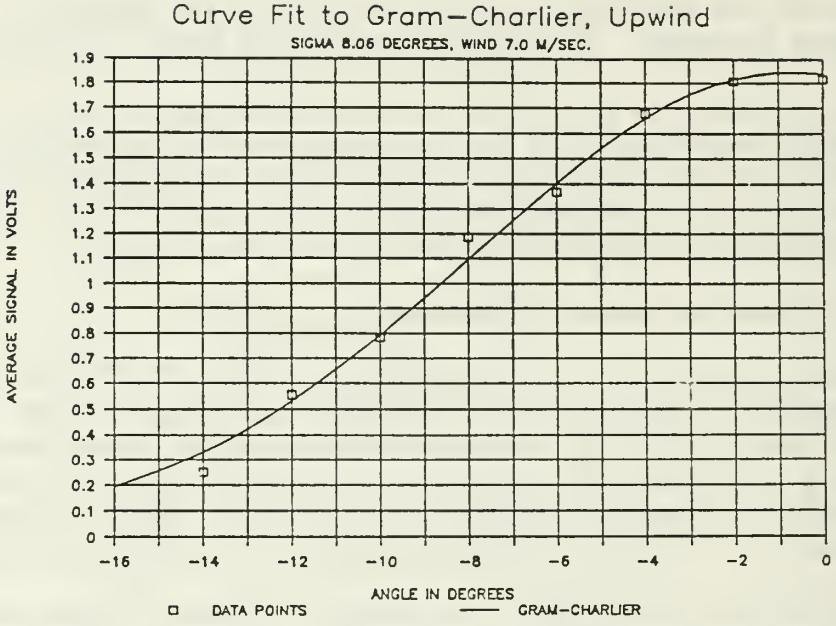

Fig. 15 Gram-Charlier upwind function fitted to the average signal values for the scan set that includes the curves of Figs. 8 to 10.

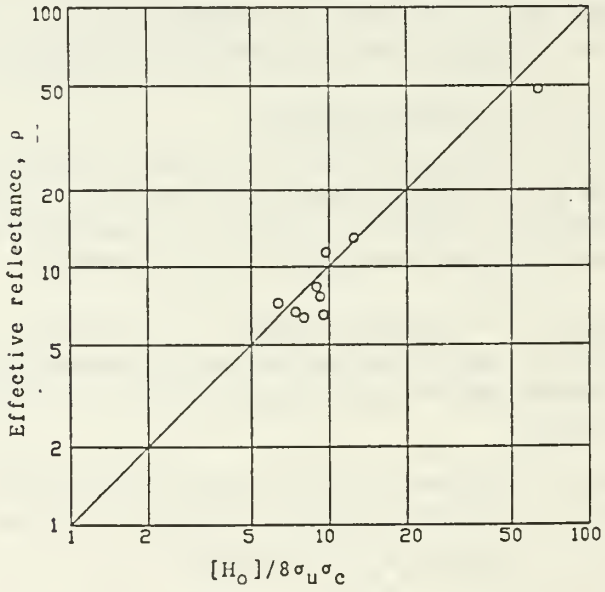

Fig. 16 Observed effective reflectance, ρ, plotted as a function of $[H_o]/8\sigma_u\sigma_c$

measured to determine the sigma values of the Gram-Charlier distribution, only a relatively few points are plotted in Fig. 16 because the earliest data were taken before the extreme effects of temperature on the laser were realized and accounted for. For the single point with high signal, for 1 December, 1989, the water surface was very little disturbed, leading to very high reflectivity. This plot is presented to indicate that the results are consistent with Cox and Munk's results.

IV. CONCLUSIONS

These results show that, for narrow beam lasers, and a sea surface including large long-wavelength waves, the reflection from the ocean surface can have a probability distribution that is antilog normal. For other surface states the distribution can range from antilog-normal through normal to log-normal. The latter seems to pertain to simpler surface states with a single set of waves generated by a long persisting wind, or for wide angle laser or radar beams, where the illuminated spot covers several of the long wavelength waves. The behavior for narrow beam lasers is favorable for application to laser altimeters, particularly those that are balloon or parachute supported and may swing about the vertical. Although the periods of zero signal will require a wait for a return signal of up to several tenths of a second, the most probable signal can be nearly the maximum and be maintained for large angles from the vertical.

LIST OF REFERENCES

1. Crittenden, E.C., Rodeback, G.W., Cooper, A.W., and Bourne, C.M., "Laser Altimeter for Use Over the Ocean", NPS Technical Report, NPS-61-89-001, April, 1989.

2. Cox, C and Munk, W., "Measurement of the Roughness of the Sea Surface from Photographs of the Sun's Glitter", Journal of the Optical Society of America, v 44, pp 838-850, November 1954.

3. Cramer, Harald, "Mathematical Methods of Statistics", Princeton University Press, Princeton, N.J., 1946.

DISTRIBUTION LIST

1.	Defense Technical Information Center Cameron Station Alexandria, VA 22304-6145	2
2.	Library, Code 524, Code 526 Naval Postgraduate School Monterey, CA 93943-5000	2
3.	Director, Research Administration, Code 81 Naval Postgraduate School Monterey, CA 93943-5000	1
4.	Prof. K. E. Woehler, Code PH/Wh Chairman, Department of Physics Naval Postgraduate School Monterey, CA 93943-5000	2
5.	Prof. E. C. Crittenden, Jr. Department of Physics Naval Postgraduate School Monterey, CA 93943-5000	2
6.	Prof. A. W. Cooper Department of Physics Naval Postgraduate School Monterey, CA 93943-5000	20
7.	Prof. G. W. Rodeback Department of Physics Naval Postgraduate School Monterey, CA 93943-5000	2
8.	Commander, Naval Sea Systems Command ATTN: PMS-405 (LCDR Carlton M. Bourne) Washington, DC 20362-5101	1
9.	Commander, Naval Sea Systems Command ATTN: SEA 06-W31 (C. Espeland) Washington, DC 20362-5101	2
10.	Commander, Naval Sea Systems Command ATTN: PMS 421 (Mr. A. Cote) Washington, DC 20362-5101	1
11.	Commander, Space and Naval Warfare Systems Command ATTN: PMW 145 Washington, DC 20362-5101	2

12. Commander, Pacific Missile Test Center 1
ATTN: Code 4030 (R. Mark)
Point Mugu, CA 93042-5000

13. U. S. Coast Guard R & D Center 2
ATTN: LCDR Miles Millbach, LT R. Engel
Avery Point, Groton, CT 06340

14. Commander, Naval Oceanographic and Atmospheric 1
Research Laboratory
ATTN: J. Cook
Naval Warfare Support Department
Monterey, CA 93943-5006

15. Commander, Naval Oceanographic and Atmospheric 1
Research Laboratory
ATTN: M. Sierchio
Naval Warfare Support Department
Monterey, CA 93943-5000

16. SPAR Aerospace Limited, 1
ATTN: Dennis Gregoris
1235 Ormond Drive
Weston, ONT, Canada, M9L 2W6

17. The Johns Hopkins University 1
Applied Physics Laboratory
ATTN: Dr. R. Steinberg
Johns Hopkins Road
Laurel, MD 20707

18. Georgia Institute of Technology Research Institute 2
Georgia Institute of Technology
ATTN: K. R. Johnson; Dr. M. Hetzler
Electromagnetics Laboratory
Atlanta, GA 30322

19. Grumman Corporate Research Center 1
ATTN: Dr. J. Krassner
Optical Physics
Bethpage, NY 11714-3580

20. Defense Research Establishment, Valcartier 2
ATTN: Electro-Optics Division
Dr. P. Chevrette, Dr. M. P. Levesque
P. O. Box 8800
Courcelette, Quebec, GOA 1RO, Canada